

Year-round record of near-surface ozone and “O₃ Enhancement Events” (OEEs) at Dome A, East Antarctica

Minghu Ding^{1,2,*}, Biao Tian^{1,*}, Michael C. B. Ashley³, Davide Putero⁴, Zhenxi Zhu⁵, Lifan Wang⁵, Shihai Yang⁶, Chuanjin Li², Cunde Xiao^{2,7}

- 5 ¹State Key Laboratory of Severe Weather, Chinese Academy of Meteorological Sciences, Beijing 100081, China
²State Key Laboratory of Cryospheric Science, Northwest Institute of Eco-Environment and Resources, Chinese Academy of Sciences, Lanzhou 730000, China
³School of Physics, University of New South Wales, Sydney 2052, Australia
⁴CNR–ISAC, National Research Council of Italy, Institute of Atmospheric Sciences and Climate, corso Fiume 4,
10 10133, Turin, Italy
⁵Purple Mountain Observatory, Chinese Academy of Sciences, Nanjing 210034, China
⁶Nanjing Institute of Astronomical Optics & Technology, Chinese Academy of Sciences, Nanjing 210042, China
⁷State Key Laboratory of Earth Surface Processes and Resource Ecology, Beijing Normal University, Beijing 100875, China
*These authors contributed equally to this work.
15 *Correspondence to:* Minghu Ding (dingminghu@foxmail.com)

Abstract. Dome A, the summit of the east Antarctic Ice Sheet, is an area challenging to access and is one of the harshest environments on Earth. Up until recently, long term automated observations from Dome A (DA) were only possible with very low power instruments such as a basic meteorological station. To evaluate the characteristics of near-surface O₃, continuous observations were carried out in 2016. Together with observations at the Amundsen-Scott Station (South Pole – SP) and
20 Zhongshan Station (ZS, on the southeast coast of Prydz Bay), the seasonal and diurnal O₃ variabilities were investigated. The results showed different patterns between coastal and inland Antarctic areas that were characterized by high concentrations in cold seasons and at night. The annual mean values at the three stations (DA, SP and ZS) were 29.2 ± 7.5 ppb, 29.9 ± 5.0 ppb and 24.1 ± 5.8 ppb, respectively. We investigated the effect of specific atmospheric processes on near-surface summer O₃ variability, when O₃ enhancement events (OEEs) are systematically observed at DA (average monthly frequency peaking up to
25 64.5% in December). As deduced by a statistical selection methodology, these O₃ enhancement events (OEEs) are affected by a significant interannual variability, both in their average O₃ values and in their frequency. To explain part of this variability, we analyzed the OEEs as a function of specific atmospheric processes: (i) the role of synoptic-scale air mass transport over the Antarctic Plateau was explored using the Lagrangian back-trajectory analysis – Hybrid Single-Particle Lagrangian Integrated Trajectory (HYSPLIT) method and (ii) the occurrence of “deep” stratospheric intrusion events was investigated using the
30 Lagrangian tool STEFLUX. The specific atmospheric processes, including synoptic-scale air mass transport, were analysed by the HYSPLIT back-trajectory analysis and the potential source contribution function (PSCF) model. Short-range transport accounted for the O₃ enhancement events (OEEs) during summer at DA, rather than efficient local production, which is consistent with previous studies of inland Antarctica. Moreover, the identification of recent (i.e., 4-day old) stratospheric

intrusions events by STEFLUX suggested that “deep” events only had a minor influence (up to 1.1 % of the period, in August) on “deep” events during the variability of near-surface summer O₃ at DA. The "deep" events during the polar night were significantly higher than those during the polar day. This work provides unique data on ozone variation at DA and expands our knowledge of such events in Antarctica. Data are available at <https://doi.org/10.5281/zenodo.3923517> (Ding et al., 2020).

Key words: near-surface O₃; Antarctica; OEE; STT;

1 Introduction

Ozone (O₃) is a natural atmospheric component that is found both in the stratosphere and troposphere and plays a major role in the atmospheric environment through radiative and chemical processes. O₃ does not have direct natural sources such as emission from the ground or vegetation, but rather is produced in the atmosphere, and its concentration ranges from a few ppb near the Earth’s surface to approximately a few ppm in the stratosphere. Stratospheric O₃, which is produced as a result of the photolysis of molecular oxygen, forms a protective layer against the UV radiation from the Sun. By contrast, throughout the troposphere and at the surface, O₃ is considered a secondary short-lived air pollutant (Monks et al., 2015), and O₃ itself is a greenhouse gas, such that a reduction in concentration has a direct influence on radiative forcing (Mickley et al., 1999; IPCC, 2013; Stevenson et al, 1998).

O₃ photochemical production in the troposphere occurs via hydroxyl radical oxidation of carbon monoxide (CO), methane (CH₄) and non-methane hydrocarbons (generally referred to as NMHC) in the presence of nitrogen oxides (NO_x) (Monks et al., 2015). As these precursors are localized and their lifetimes are generally short, the distribution of near-surface O₃, which is produced from anthropogenic precursors, is also localized and time-variant. In the presence of strong solar radiation with $\lambda < 424$ nm, volatile organic compounds (VOCs) and NO_x (NO + NO₂), O₃ is photochemically produced and can accumulate to a hazardous level during favourable meteorological conditions (Davidson, 1993; Wakamatsu et al., 1996). In the case of NO_x-rich air, NO₂ is produced and accumulates via the reaction between NO and HO₂ or RO₂ (peroxy radicals), which is followed by the accumulation of O₃. However, in the case of NO_x-poor air, these proxy radicals react with O₃ and lead to O₃ loss (Lin et al., 1988). Experiments conducted in Michigan (Honrath et al., 2000a) and Antarctica (Jones et al., 2000) found that NO_x can be produced in surface snow. This production appears to be directly driven by incident radiation and photolysis of nitrate deposited in the snow (Honrath et al., 2000a, b).

Previous studies have shown that the near-surface O₃ of Antarctica may be influenced by a number of climate-related variables (Berman et al., 1999), such as the variation of UV flux caused by the variation of O₃ column concentration over Antarctica (Jones and Wolff, 2003; Frey et al., 2015), the accumulation and transport of long-distance, high concentration air masses (e.g., Legrand et al., 2016), and the depth of continental mixing layers. Many studies have observed summer episodes of “O₃ enhancement events” (OEEs) in the Antarctic interior (e.g., Crawford et al., 2001; Legrand et al., 2009; Cristofanelli et al., 2018), and they attributed this phenomenon to the NO_x emissions from snowpack and subsequent photochemical O₃

65 production (for example, Jones et al., 2000). Moreover, this may provide an input source for the entire Antarctic region (for
example, Legrand et al., 2016; Bauguitte et al., 2011). As the solar irradiance and the nitrate aerosol concentration increase, the
emission of NO_x will increase through the photodenitrification process of the summer snowpack (e.g. $\text{NO}_3 + h\nu \rightarrow \text{NO}_2 + \text{O}$;
 $\text{O} + \text{H}^+ \rightarrow \text{OH}$; Honrath et al., 2000; Warneck et al., 1989). Helmig et al. (2008a,b) provided further insight into the vigorous
70 photochemistry and O_3 production that result from the highly elevated levels of NO_x in the Antarctic surface layer. During
stable atmospheric conditions, which are typically observed during low wind and fair sky conditions, O_3 accumulated in the
surface layer can reach up to twice its background concentration. Neff et al. (2008a) showed that shallow mixing layers
associated with light winds and strong surface stability can be among the dominant factors leading to high NO levels. As
shown by Cristofanelli et al. (2008) and Legrand et al. (2016), the photochemically-produced O_3 in the PBL over the Antarctic
Plateau can affect the O_3 variability thousands of km away from the emission area, due to air mass transport.

75 The near-surface O_3 concentrations at high-elevation sites can also be increased by the downward transport of O_3 -rich air from
the stratosphere during deep convection and stratosphere-to-troposphere transport (STT) events. Moreover, the stratospheric
 O_3 in the polar regions can be transferred to the troposphere not only during intrusion events but also as a result of slow but
prolonged subsidence (e.g., Gruzdev et al., 1993; Roscoe et al., 2004; Greenslade et al. 2017). The earliest studies, carried out
by the aircraft flight NSFC-130 over the Ellsworth Mountains of Antarctica in 1978, found that mountainous terrain may
80 induce atmospheric waves that propagate through the tropopause. The tropospheric and stratospheric air may be mixed,
leading to an increase in the tropospheric O_3 concentration (e.g., Robinson et al., 1983). Radio soundings at the Resolute and
Amundsen-Scott Stations also showed the existence of transport from the stratosphere to the troposphere, and the flux could
reach up to 5×10^{10} mol/cm²/s (e.g., Gruzdev et al., 1993). Recently, Traversi et al. (2014, 2017) suggested that the variability of
air mass transport from the stratosphere to the Antarctic Plateau could affect the nitrate content in the lower troposphere and the
85 snowpack.

Currently, the climatology of tropospheric O_3 over Antarctica is relatively understudied because observations of year-round
near-surface O_3 have been tied to manned research stations. These stations are generally located in coastal Antarctica, except
for the South Pole (SP) and Dome C continental stations on the East Antarctic Plateau. Thus, the only information currently
available for the vast region between the coast and plateau are spot measurements of boundary layer O_3 during summer from
90 scientific traverses (e.g., Frey et al., 2015) or airborne campaigns (e.g., Slusher et al., 2010). Moreover, the vertical profile of
 O_3 in the troposphere cannot be measured by satellites because the high density of O_3 in the stratosphere leads to the inaccurate
estimation of tropospheric O_3 by limb-viewing sensors. Estimates of total O_3 in the troposphere have been made by subtracting
the stratospheric O_3 column (determined by a limb-viewing sensor) from the total column of O_3 (measured by a nadir-viewing
sensor) (Fishman et al., 1992). In other words, tropospheric profiles cannot be obtained by satellites, and we cannot examine
95 the spatial distribution of near-surface O_3 from space. As a result of these limitations, a dearth of information exists regarding
the spatial gradient of near-surface O_3 across Antarctica and how it varies throughout the year.

To better understand the spatial variations and the source-sink mechanisms of near-surface O₃ in Antarctica, near-surface O₃ concentrations were measured during 2016 at Dome A (DA) and the Zhongshan Station (ZS). Together with records from the Amundsen-Scott Station (SP), we analysed specific processes that affect the intra-annual variability in surface O₃ over the East Antarctic Plateau; in particular, we determined (i) the synoptic-scale air mass transport within the Antarctic interior and (ii) the role of STT transport. This study broadens the understanding of the spatial and temporal variations in the near-surface O₃ concentration and transport processes that impact tropospheric O₃ over high plateaus.

2 Sites and methods description

2.1 Near-surface ozone observations

There are several methods to measure the concentration of ozone, including ultraviolet spectrophotometry, iodometry, sodium indigo disulfonate spectrophotometry, gas chromatography, chemiluminescence, fluorescence spectrophotometry and long optical path differential absorption spectrometry, etc. (e.g. Wang et al., 2017). Of them the ultraviolet spectrophotometry is the most popular for the surface ozone monitoring and applied into many commercial instruments. The common ones such as Thermo 49C (Liu et al., 2006), API 400E (Sprovieri et al., 2003), ESA O342M (Lei et al., 2014), Ecotech 9810B (Moura et al., 2011), have been used in many regions for their larger measuring range and high precision, but they are expensive, need plenty of power supply and regular maintenance. Recently, more and more studies chose the portable ozone monitors such as Model 205, Aeroqual Series 500, POM, due to its advantages of small volume, low price, low energy consumption and good applicability for field observation (e.g. Johnson et al., 2014; Lin et al., 2015; Sagona et al., 2018). In Antarctica, only few stations have carried out continuous ozone monitoring and all of them were equipped with the common types, that is Thermo/Ecotech types, as we know.

The Kunlun Station (80°25'02"S, 77°06'59"E, altitude 4087 m) is located in the DA area, on the summit of the east Antarctic Ice Sheet (Figure 1). The only continuous power supply is the PLATO-A observatory, which can also provide internet access via the Iridium satellite network (detailed introduction of PLATO observatory can be found in Lawrence et al. (2009)). Due to the limitation of energy consumption and conditions encountered during transportation from coast to the Dome, larger monitors such as Thermo 49i cannot be used. Thus, on the 1st of Jan 2016, we deployed a Model 205 Dual Beam Ozone Monitor (205 2B) during the 33rd Chinese National Antarctic Research Expedition. The instrument has been certified by Environmental Protection Agency and makes use of two detection cells to improve its precision, baseline stability, and response time. In the dual beam instrument, UV light intensity measurements I_0 (O₃-scrubbed air) and I (unscrubbed air) are performed simultaneously (Wang et al., 2017). And it is the fastest UV-based O₃ monitor till now, with a small size, light weight, and low power requirements (Supplementary-Table S1). Especially, quick response is particularly desirable for unattended stations, aircraft and balloon measurements. In Dome A, we use Teflon pipeline to connect the free air at ~4m

above surface with the instrument. At the inlet of the pipeline, a Thermo 47mm filter was used to prevent snow particles. During the observation, the instrument was set at the sampling frequency of once an hour, and the data was transmitted to the observatory computer through RS232 and sent to Beijing by satellite.

130 The Zhongshan Station (69°22'12"S, 76°21'49"E, altitude 18.5 m) is located at the edge of the east Antarctic Ice Sheet (Figure 1). The atmospheric chemistry observatory was constructed at the Swan Ridge, northwest of the Nella fjord, at where we installed a UV absorption near-surface O₃ analyzer (EC9810A) for long-term near-surface O₃ monitoring in Jan. 2008. The air inlet was 4 m above the surface, and connected to the analyzer through the Teflon pipe. The observational frequency was 3 min, and the data were transferred in real time to Beijing. Furthermore, to prevent data losses, a CR1000 data logger was used to
135 record the data output in real time. Every three months, the O₃ analyzer was calibrated using the EC9811 O₃ calibrator, and 5 standard concentrations of O₃ gas were generated for each calibration. The calibration concentration and measured concentration underwent correlation analysis, and seasonal calibration results were generated every three months. In 2016, 5 calibrations were made, and the appropriate correlation coefficients (r) were all greater than 0.9995.

The Amundsen-Scott Station (89°59'51.19 "S, 139°16'22.41" E, altitude 2835 m) is located at the SP and operated by the
140 United States. In 2016, an Thermo 49C ozone monitor was used and 5-minute and 1-hour data was uploaded to GAW (Global Atmospheric Watch) every month. The record used in this paper was downloaded from the Earth System Research Laboratory Global Monitoring Division under the NOAA (<https://www.esrl.noaa.gov/gmd/dv/data>).

The hourly data of these stations collated here are available at <https://doi.org/10.5281/zenodo.3923517> (Ding et al., 2020).

2.2 Calibration process and results

145 Generally, the zero point, span point and operation parameters of the O₃ monitor should be checked before each operation. The zero point should be checked regularly during continuous observation. While such regular calibration was done at the Global Atmosphere Watch (GAW) and Zhongshan Station, it was not possible at DA due to the lack of logistic support and the extreme environment. To minimize the error and evaluate the accuracy of the experiment, a UV-absorption O₃ calibrator Thermo 49i-PS was used to examine the Model 205. The calibration procedure follows China's environmental protection
150 standard "ambient air - Determination of ozone - ultraviolet method" (HJ590-2010) (http://www.mee.gov.cn/gkml/sthjbgw/sthjbgg/201808/t20180815_451411.htm) which is more strict than USEPA (Ref: USEPA. Quality Assurance Handbook for Air Pollution Measurement Systems Volume II: Ambient Air Quality Monitoring Program[EB/OL].[2008-12-01]. <http://www.epa.gov/ttn/amtic/files/ambient/pm25/qa/QAHandbook-Vol-II.pdf>): the slope of calibration curve ranges between 0.95-1.05, and the intercept ranges between -5-5 ppb. Instruments used in the calibration
155 process include a DOA-p512-bn air compressor (USA), in addition to the Thermo 49ips O₃ calibrator and the Model 205 O₃ monitor. Before each test, the O₃ calibrator and the O₃ monitor were turned on and preheated for 12 hours, and the measuring range was set to 400 ppb. We first generate a zero concentration using the Thermo 49ips and, once the analyzer response has stabilized on zero reading, we adjusted the Model 205's internal zero setting to matches the zero air source. Then, O₃ airflow at

400 ppb level was generated and injected into the analyzer, and a correction factor was calculated based on the observed value,
160 which was then loaded into the Model 205 configuration.

After the calibration of the internal zero/span settings, a second stage of calibration was performed involving multi-point
verification to check the response and stability of the analyzer. On Oct 5th 2015 (before the instrument was shipped) and May
6th 2017(the day that the instrument was transported back from Antarctica), a zero and 7 upscale points (0, 20, 35, 50, 65, 80,
100, 120 ppb) encompassing the full scale of the observation range (Table 1), were generated by the Thermo 49ips to test the
165 Model 205 analyzer. Each point was observed for 15 min, during the last 10 minutes of which readings were taken every
minute of the calibrator and analyzer. Based on this experiment, the slope and intercept of the calibration curve were calculated
by least squares. The results are shown in Table 2, it can be concluded that the slopes of the linear correction curve were
0.99936 and 1.02520, and the intercepts were 0.53861 and 0.852201, which fulfilled the requirements of HJ590-2010 and
USEPA.

170 Another challenge when monitoring the atmosphere is the stability of the analyzer, which includes the analyzer's response time.
Similarly with the regular calibration, it could not be performed during the observation period, but it was reassuring that the
Model 205 was still in good condition when we did the multi-point verification in May 2017, as shown in Table 2. The slope
and intercept of the two calibration curves changed little and the standard uncertainties were small. To further test the stability,
data consistency was also examined and the mean absolute deviation between two adjacent values was only 0.09 ppb. The
175 largest difference was 0.61 ppb, indicating that the analyzer was stable and reliable.

Before analysis, a variance test was used to remove abnormal data based on the Laida criterion method, which assumes that the
records obeyed a normal distribution. The formula is $|x_i - \bar{x}| > 3\sigma$, where x_i is the measured value, \bar{x} is the time series
mean and σ is the standard deviation. After processing, 99.3%, 99.6%, and 89.3% of the hourly mean data were retained from
the Amundsen-Scott Station, Zhongshan Station and Kunlun Station, respectively.

180 **2.3 Air mass back-trajectory calculations**

Gridded meteorological data for backward trajectories in Hybrid Single-Particle Lagrangian Integrated Trajectory (HYSPLIT)
were obtained from the Global Data Assimilation System (GDAS-1) operated by the U.S. National Oceanic and Atmospheric
Administration (NOAA) with $1^\circ \times 1^\circ$ horizontal resolution and 23 vertical levels, from 1000 hPa to 20 hPa
(<http://www.arl.noaa.gov/gdas1.php>).

185 The HYSPLIT backward air mass trajectory model was previously applied to atmospheric research in Antarctica (Legrand et
al., 2009; Hara et al., 2011). We used the HYSPLIT model in this paper to analyse the impact of varying air mass sources and
the intrusion of stratospheric O₃. Backward trajectories and clusters were calculated using the US National Oceanic and
Atmospheric Administration (NOAA)-HYSPLIT model (Draxler and Rolph, 2003; <http://ready.arl.noaa.gov/HYSPLIT.php>),
which is a free software plug-in for MeteoInfo (Wang, 2014; <http://meteothink.org/>). The backward trajectories starting height

190 was set at 20 m above the surface and the total run times was 120 hours for each backward trajectory, and each run was performed in time intervals of 6 hours (00:00, 06:00, 12:00, 18:00).

The integral error part of the trajectory calculation error can be estimated by simulating the backward trajectory at the end of the forward trajectory and comparing the differences of the tracks. The starting point of the backward integration is set as (77.12 ° E, 80.42 °S, 20m a.g.l.), the backward integration is 120 hours. Then the point reached at this time is taken as the
195 starting point, and a forward simulation is made for 120h. In this simulation experiment, the contribution of integration error to trajectory calculation error is very small within the first 72 hours. With the extension of integration time, the integration error slightly increases.

The air mass trajectories were assigned to distinct clusters according to their moving speed and direction using a k-means clustering algorithm (Wong, 1979). Concerning with this study focused on transport pathway of O₃, the clustering result with
200 the smallest number was selected as done by Wang et al. (2014). It was found three clusters performance best to represent the meteorological characteristics of the transport pathways at DA. This number was then selected as the expected number of air mass trajectory clusters. A more detailed clustering procedure using the k-means algorithm can be found in Wang et al. (2014).

2.4 Potential source contribution function

The observation of a secondary maximum of O₃ in November–December at the inland Antarctic sites was first reported for the
205 SP by Crawford et al. (2001), and was attributed to photochemical production induced by high NO_x levels in the atmospheric surface layer, which were generated by the photo-denitrification of the Antarctic snowpack (same as Davis et al., 2001). At DC, a secondary maximum in November–December 2007 was also reported by Legrand et al. (2009), proving that photochemical production of O₃ in the summer takes place over a large part of the Antarctic Plateau. A further study by Legrand et al. (2016) found that the highest near-surface O₃ summer values were observed within air masses that spent extensive time over the
210 highest part of the Antarctic Plateau before arriving at DC. To investigate the possible influence of synoptic-scale air mass circulation on the occurrence of OEEs at DA, 5-day HYSPLIT back-trajectories were analyzed (Figure 9). We used the potential source contribution function (PSCF, see, e.g., Hopke et al., 1995; Brattich et al., 2017) to calculate the conditional probabilities and identify the geographical regions related to the occurrence of NOEEs and OEEs at DA (Figure 7).

As in Yin et al. (2017), the potential source contribution function (PSCF) assumes that back trajectories arriving at times of
215 high concentrations likely point to significant pollution directions (Ashbaugh et al., 1985). This function was often applied to locate air masses associated with high levels of near-surface O₃ at different sites (Kaiser et al., 2007; Dimitriou and Kassomenos, 2015). In this study, the PSCF was calculated using HYSPLIT trajectories. The top of the model was set to 10000 m a.s.l. The PSCF values for the grid cells in the study domain were calculated by counting the trajectory segment endpoints that terminated within each cell (Ashbaugh et al., 1985). If the total number of end points that fall in a cell is n_{ij} and there are m_{ij}
220 points for which the measured O₃ parameter exceeds a criterion value selected for this parameter, then the conditional probability, the PSCF, can be determined as

$$PSCF_{ij} = \frac{m_{ij}}{n_{ij}} \quad (1)$$

The concentrations of a given analyte greater than the criterion level are related to the passage of air parcels through the ij th cell during transport to the receptor site. That is, cells with high PSCF values are associated with the arrival of air parcels at the receptor site, which has near-surface O₃ concentrations that are higher than the criterion value. These cells are indicative of areas with ‘high potential’ contributions of the constituent. Identical PSCF_{ij} values can be obtained from cells with very different counts of back-trajectory points (e.g., grid cell A with $m_{ij} = 5000$ and $n_{ij} = 10000$ and grid cell B with $m_{ij} = 5$ and $n_{ij} = 10$). In this extreme situation, grid cell A has 1000 times more air parcels passing through it than grid cell B. Because the particle count in grid cell B is sparse, the PSCF values in this cell are highly uncertain. To explain and expound the uncertainty due to the low values of n_{ij} , the PSCF values were scaled by a weighting function W_{ij} (Polissar et al., 1999). The weighting function reduced the PSCF values when the total number of endpoints in a cell was less than approximately 3 times the average number of end points per cell. In this case, W_{ij} was set as follows:

$$W_{ij(NOEE)} = \begin{cases} 1.00 & nij > 12Nave \\ 0.70 & 12Nave > nij > 3Nave \\ 0.42 & 3Nave > nij > 1.5Nave \\ 0.05 & Nave > nij \end{cases} \quad (2)$$

$$W_{ij(OEE)} = \begin{cases} 1.00 & nij > 8Nave \\ 0.70 & 8Nave > nij > 2Nave \\ 0.42 & 2Nave > nij > 1Nave \\ 0.05 & Nave > nij \end{cases} \quad (3)$$

where $Nave$ represents the mean n_{ij} of all grid cells. The weighted PSCF values were obtained by multiplying the original PSCF values by the weighting factor.

3 Near-surface O₃ variability

3.1 Mean concentration

At the DA, SP, and ZS sites, the annual mean concentrations of near-surface O₃ were 29.2 ± 7.5 ppb, 29.9 ± 5.0 ppb and 24.1 ± 5.8 ppb, respectively; the maximum annual mean concentration reached 42.5 ppb, 46.4 ppb and 32.8 ppb, respectively; and the minimum annual mean concentrations were 14.0 ppb, 10.9 ppb and 9.9 ppb, respectively. The inland stations are characterized by higher annual mean concentrations than the coastal station.

There were also obvious differences between polar day and polar night at all stations. In Figure 2, we define the polar day and night windows by the day of year margins and have used different shading colours to identify the polar day and polar night. The average concentrations of near-surface O₃ during polar night at the DA, SP and ZS sites were 34.1 ± 4.3 ppb, 31.5 ± 3.9 ppb and 28.7 ± 1.3 ppb, respectively, and much lower concentrations appeared during non-polar night, with corresponding values of 26.1 ± 7.0 ppb, 28.1 ± 5.8 ppb and 23.1 ± 5.9 ppb, respectively. Interestingly, the SP had the highest near-surface O₃ concentration during non-polar night, whereas at DA the highest concentration occurred during polar night and the largest variation occurred at this site.

250 3.2 Seasonal variation

In this part, we define Oct-Mar as the warm season and Apr-Sep as the cold season, which is similar to the definition of polar day and night.

In agreement with previous studies (Oltmans et al., 1976; Gruzdev et al., 1993; Ghude et al., 2005), the concentrations of near-surface O₃ at the three stations were high and less variable during the cold season and low and more variable during the warm season (Figure 3). In Antarctica, the emissions of O₃ precursors are generally less than those at mid and low latitudes, whereas ultraviolet radiation is relatively strong; thus, when solar radiation occurs, the depletion effect is much greater than the effects from photochemical reactions during the warm season (Schnell et al., 1991). As explained by previous studies, during the polar night, due to the lack of light, the photochemical reactions stop. Moreover, due to the lack of loss effect, the O₃ concentration gradually increased and the fluctuations became smaller. During the polar night, the monthly variation of surface O₃ at ZS was lower than that at the DA but higher than that at the SP. However, due to strong UV radiation in the low latitude areas and the presence of bromine-controlled O₃ depletion events in coastal areas, the ZS shows a large seasonal variations during the non-polar night (Wang et al., 2011; Prados-Roman et al., 2017). However, at the SP Station, the largest standard deviation was observed in December, similarly to the characteristics at Dome-C station (DC) from November to December (Legrand et al., 2009; Cristofanelli et al., 2018). Figures 2 and 3 indicate that the near-surface O₃ showed obviously larger variations at the DA than the SP during the polar night, since, due to the different geographical location, the meteorological conditions of DA and SP are different. The abnormal fluctuation of O₃ concentration over the DA during the polar night may be related to its special geographical environment.

As mentioned in the introduction section, mountainous topography/mountain waves may disturb advection transport in the stratosphere and lead to downward transportation to the troposphere (Robinson et al., 1983). DA is on the summit of the east Antarctic Ice Sheet, and the tropospheric depth is only ~4.6 km (Liang et al., 2015), which favours exchange between the stratosphere and troposphere. However, the topography in this area is very flat and creates a disadvantage for mountain waves. Does O₃ transport occur? We will analyse and discuss this question in section 4.

3.3 Diurnal variation

To characterize the typical monthly O₃ diurnal variations at the three stations, we analysed the mean diurnal variations of O₃ at the three stations (Figure 4) and the standard deviation of the mean diurnal variations (Figure 5). At the DA site, the mean diurnal concentrations for each month were relatively steady, with the standard deviation of the mean diurnal concentration for each month being lower than 0.4 ppb. At the SP, the mean diurnal concentrations were less variable as well. Except for December, the standard deviation of the mean diurnal concentration was lower than 0.3 ppb. At ZS, except for October, the standard deviation of the mean diurnal concentration was greater than that at the other two stations. In particular, the standard deviation of the mean diurnal concentration of ZS in September, November and December exceeded 0.5 ppb. Obviously, the average daily concentration fluctuation in Zhongshan station was obviously different with the two inland stations, which can be attributed into their background climates. In Spring, ODEs occur frequently at Zhongshan Station. And this phenomenon always accompanies with abrupt weather transit from continental dominant to oceanic dominant, in other words, the BrO brought by northerly wind from sea ice area could lead to serious ozone depletion (Wang Y et al., 2011; Ye et al., 2018). Whereas at inland stations like DA and SP, there were rarely ODEs.

On the whole, the mean diurnal variations in different time periods were not obvious, and the mean diurnal concentrations of the three stations fluctuated within a range of less than 1 ppb. The magnitude of the diurnal variation was low, which is similar to the variations of other Antarctic stations, Neumayer and Marambio for instance (Nadzir et al., 2018).

4 Ozone under OEEs at the Kunlun Station

4.1 Identification of OEEs

Our method to select the days characterized by OEEs is based on the procedure used in Cristofanelli et al. (2018). First, a sinusoidal fit is used to calculate the O₃ annual cycle not affected by the OEEs, then a probability density function (PDF) of the deviations from the sinusoidal fit is calculated, with the application of a Gaussian fit to the obtained PDF. As reported in Giostra et al. (2011), the deviations from the Gaussian distribution (calculated by using the Origin 9© statistical tool) can be used to identify observations affected by non-background variability. We computed the further Gaussian fitting of PDF points beyond 1 σ (standard deviation) of the Gaussian PDF, and determined the non-background O₃ daily values that may be affected by "anomalous" O₃ enhancement. The intersection of the two fitting curves is taken as our screening threshold (3.4 ppb at SP, 3.4 ppb at DA and 2.5 ppb at ZS). Figures 6a, 6b and 6c show OEE days and NOEE days at these three stations, while Figures 6d, 6e and 6f report the distribution frequency of OEE days.

In total, 42 days at DA were found to be affected by anomalous OEEs: 14.3% in January, 2.4% in May, 14.3% in June, 4.8% in July, 11.9% in August, 4.8% in November and 47.6% in December (Figure 6e, blue bars). This result clearly indicates that half of the anomalous days occurred in December, followed by January and June. At SP, 36 days with OEEs were found in 2016:

44.4% in January, 30.6% in November, and 25% in December (Figure 6d, grey bars). Apparently, OEEs occur only in summertime at this measurement site. ZS was characterized by more days with OEEs: 53 days in April (34.0%), followed by September (18.9%), January (13.2%), October (11.3%), November (11.3%), December (5.7%) March (3.8%) and May (1.9%) (Figure 6f, yellow bars).

From the results above, it can be seen that SP was characterized by concentrated OEE occurrences, and ZS had the most scattered OEEs pattern. In addition, all OEEs at SP and ZS occurred during the Antarctic warm season, and no OEEs were present during the polar night, similarly to the pattern observed at DC (Cristofanelli et al., 2018). In contrast, the OEEs also occurred during the polar night in DA, and the number of OEE occurrence days accounted for up to 33% of the total number of events throughout the year. This is the main reason of the large variations of daily average concentration during the polar night of DA.

Previous studies (e.g., Legrand et al., 2016; Cristofanelli et al., 2018) carried out in DC showed that the O₃ variability at DC could be associated with processes occurring at long temporal scales. In addition, the accumulation of photochemically produced O₃ during transport of air masses was the main reason for OEEs, whereas the stratospheric intrusion events had only a minor influence on OEEs (up to 3%). This finding cannot explain the temporal occurrence pattern of OEEs at DA. To determine the unknown cause, we investigated the synoptic-scale air mass transport and the STT occurrence at the measurement site.

4.2 Role of synoptic-scale air mass transport

During NOEEs, the air masses arriving at DA mainly come from the west and east of DA, and the 3-D clusters show that the air masses travelled over the Antarctic plateau before reaching DA (Figure 8b). The difference in the number of the three cluster trajectories is small, and the difference in the corresponding cluster average concentrations is not large. Using the PSCF results, we have identified air masses associated with higher surface ozone at DA during NOEEs (Figure 8a). The Antarctic Plateau to the east and west of DA had high PSCF weight values (Figure 7), which shows that, during NOEEs, the potential source area of surface O₃ for DA is mainly in the inland plateaus in the east and west, and the area of high PSCF weight values distribution in the east is more larger than other directions.

Compared with NOEEs, the clustering results of trajectories during OEEs have different characteristics. In OEEs, the air masses that arrived at DA were prevalent from the north and from the west, and the 3-D clusters indicated that the 73% of the air mass trajectories came from the area north of DA (red line in Figure 8e). The average concentrations of the three clusters differ greatly (Figure 8f), but they are all higher than those obtained for NOEEs. It should be noted that 68% of Line-2 cluster (green line in Figure 8d) occurred during the polar night (Figure 9) and had a high average O₃ concentration (reached 36.3 ppb). This shows that the OEEs of the polar night are more affected by the high value O₃ air masses over the plateau west of DA than those during the polar day. Using the PSCF results, during OEEs, we did not find a large area of high WPSCF value, the high WPSCF value only appeared in the east and the north of DA over a limited area. However, independently on the polar day or on

335 the polar night, the Line-1 cluster trajectory accounted for more than 60% during OEEs. In addition, the short distance of
Line-1 cluster trajectory indicates that the air mass transport speed is slow, which is conducive to the accumulation of O₃ along
the way. It can be seen from Figure 8e that the characteristic values of backward trajectory clustering during OEEs are mostly
lower than 200 m a.g.l. (supporting the role of snow as the source of near surface O₃). As Fiebig et al. (2014) has proposed, the
increase of O₃ values in the near surface of central Antarctica may also be related to the transport of free tropospheric air and
aged pollution plumes from low latitudes. In addition, Figure 10 shows that the average O₃ growth rate reached 0.29 ppb/h
340 during OEEs in polar night, while the average O₃ growth rate was -0.06 ppb/h during NOEEs in polar night (Figure 10). The
statistical scatter distribution showed that 97% of OEEs occurred when the wind speed was lower than 4 m/s. The overall
average wind speed during OEEs is also significantly lower than that of NOEEs. As Helmig et al. (2008a) have proposed,
during stable atmospheric conditions (which typically existed during low wind and fair sky conditions) ozone accumulates in
345 the surface layer and its concentration increases rapidly.

This finding confirms that the OEEs of DA are mainly caused by the accumulation of high concentrations of air masses
transported occurring nearby, and the synoptic-scale transport can favor the photochemical production and the accumulation of
O₃ accumulation by air masses travelling over the plateau near the north of DA before their arrival.

4.3 Role of STT events

350 4.3.1 Identification of “deep” STT events

Several methods can be applied to study stratosphere-to-troposphere transport (STT) events. One method is the
chemistry-climate hindcast model GFDL-AM3, which Lin et al. (2017) used to evaluate the increasing anthropogenic
emissions in Asia, and Xu et al. (2018) used to examine the impact of direct tropospheric ozone transport at the Waliguan
Station. Stratosphere-to-Troposphere Exchange Flux (STEFLUX, Putero et al., 2016) is a novel tool to quickly obtain reliable
355 identification of STT events occurring at a specific location and during a specified time window. STEFLUX relies on a
compiled stratosphere-to-troposphere exchange climatology, making use of the ERA-Interim reanalysis dataset from the
ECMWF, and a refined version of a well-established Lagrangian methodology. STEFLUX is able to detect stratospheric
intrusion events on a regional scale, and it has the advantage of retaining additional information concerning the pathway of
stratosphere-affected air masses, such as the location of tropopause crossing and other meteorological parameters along the
360 trajectories.

We applied STEFLUX to assess the possible contribution of STT to near-surface O₃ variability in the DA region (i.e.,
STEFLUX “target box”, for further details on the methodology see Putero et al., 2016), and for identifying the measurement
periods possibly affected by “deep” STT events (i.e., stratospheric air masses transferred down to the lower troposphere). For
this work, we set the top lid of the box at 500 hPa, and the following geographical boundaries: 79–82 °S, and 76–79 °E. A
365 “deep” STT event at Kunlun Station was determined if at least 1 stratospheric trajectory crossed the 3-D target box.

4.3.2 Role of STT events at DA

The possible occurrence of stratospheric intrusion events, and their role in affecting the variability of near-surface O₃ and tropospheric air-chemistry in Antarctica has been investigated in several studies (Murayama et al., 1992; Roscoe, 2004; Stohl and Sodemann, 2010; Mihalikova and Kirkwood, 2013; Traversi et al., 2014; Traversi et al., 2017; Cristofanelli et al., 2018).

370 To provide a systematic assessment of the possible influence of “deep” STT events to the near-surface O₃ variability at Kunlun Station, we used the STEFLUX tool (see Sect. 4.3.1). Figure 11 shows the distribution of the occurrence of “deep” STT events over DA during the year. Although it is difficult to see a clear seasonal cycle, due to the low frequency of “deep” STT events, our results are in agreement with previous studies, indicating STT influence of up to 2% on a monthly basis (Stohl and Sodemann, 2010; Cristofanelli et al., 2018). According to our STEFLUX outputs, the highest frequency of “deep” STT events
375 was observed in May and August (1.1%). The frequency of occurrence of “deep” STT events identified by STEFLUX at Kunlun Station is about one order of magnitude lower than the occurrence of OEEs. Thus, a direct link of STT with OEEs interannual variability is unlikely, as also reported for DC station (Cristofanelli et al., 2018). Nevertheless, STT events can be a source of nitrates for the Antarctic atmosphere through different processes, thus indirectly affecting near-surface O₃ concentrations and favouring the presence of OEEs (Traversi et al., 2014; 2017).

380 5 Summary

Based on the in-situ monitoring data during 2016 at DA, the variation, formation, and decay mechanisms of near-surface O₃ were studied and compared with those at SP and ZS stations. The annual mean concentrations of near-surface O₃ at the DA, SP and ZS sites were 29.2 ± 7.5 ppb, 29.9 ± 5.0 ppb, and 24.1 ± 5.8 ppb, respectively. The near-surface O₃ concentrations were clearly higher in winter/polar night, with small fluctuations, than in the other seasons, which is different from the patterns
385 observed at low latitudes. The O₃ in inland areas was also higher than over the coast.

The diurnal variations showed nonsignificant regular patterns, and the range of the average diurnal concentration fluctuation was less than 1 ppb at all three stations. These findings suggest that the synoptic transport somehow controls the overall O₃ variability, as has been shown at the SP and DC stations (Neff et al., 2008b; Cristofanelli et al., 2018).

At Kunlun station, it is unlikely that there is a direct relationship between STT and OEEs. The frequency of deep STT events
390 identified by STEFLUX is about an order of magnitude lower than OEEs, and reaches its highest frequency (1.1%) in May and August. As deduced by the STEFLUX application, “deep” STT events play a marginal role in steering the occurrence of OEEs at DA via “direct” transport of O₃ from the stratosphere/the free troposphere, to the surface. As explained in Cristofanelli et al. (2018), this can be related to an underestimation of STT “young” (i.e., < 4-day old) events by STEFLUX, or to insufficient spatial and vertical resolution from ERA-Interim to fully resolve the complex STT transport in the Antarctic atmosphere
395 (Mihalikova and Kirkwood, 2013). Despite this, STT can still represent a source of nitrates for the Antarctic snowpack, thus

possibly affecting summer photochemical O₃ production. Therefore, it is important to carry out further studies to better assess these processes.

The characteristics and mechanisms of near-surface O₃ revealed in this paper have important implications for better understanding the formation and decay processes of near-surface O₃ in Antarctica, especially over the plateau areas.

400 Nevertheless, the lack of observations restricted our ability to amass more information. Long-term sustained observations at Dome A, Dome C, Dome F, SP, Vostok, and other locations, would greatly help in the future.

6 Data availability

All data presented in this paper are available in <https://doi.org/10.5281/zenodo.3923517> (Ding et al., 2020). The data set covers the hourly average concentrations of near-surface ozone at three stations (i.e. SP, ZS, DA).

405 Author contribution

Minghu Ding and Biao Tian designed the experiments and wrote the manuscript; Minghu Ding carried out the experiments; Biao Tian analyzed the experimental results. Minghu Ding, Biao Tian and Davide Putero revised the manuscript; Davide Putero run the STEFLUX tool. Michael Ashley, Zhenxi Zhu, Lifan Wang, Shihai Yang, Jie Tang, Chuanjin Li, Cunde Xiao and discussed the results.

410 Acknowledgements:

This work is financially supported by the National Natural Science Foundation of China (41771064), the Strategic Priority Research Program of Chinese Academy of Sciences (XDA20100300) and the Basic Fund of the Chinese Academy of Meteorological Sciences (2018Z001). The observations were carried out by during the Chinese National Antarctic Research Expedition at the Zhongshan Station and the Kunlun Station. We are also grateful to NOAA for providing the HYSPLIT model and GFS meteorological files. Yaqiang Wang is the developer of MeteoInfo and provided generous help for the paper. PLATO-A was supported by the Australian Antarctic Division and with NCRIS funding through Astronomy Australia Limited.

References

Ashbaugh, L. L., Malm, W. C., and Sadeh, W. Z.: A residence time probability analysis of sulfur concentrations at Grand
420 Canyon National Park, *Atmos. Environ.*, 19, 1263–1270, [https://doi.org/10.1016/0004-6981\(85\)90256-2](https://doi.org/10.1016/0004-6981(85)90256-2), 1985.

- Bauguitte, S. J. B. , Jones, A. E. , Hutterli, M. A. , Anderson, P. S. , Maxfield, D. J. , Roscoe, H. K. , Wolff, E. W. , Virkkula, A. , Kirkwood, S. and Weller, R. : Preliminary data analysis from the IPY autonomous surface ozone monitoring network in Dronning Maud Land, Antarctica , EGU General Assembly , 2009.
- 425 Berman S., Ku J Y., Rao S T.: Spatial and Temporal Variation in the Mixing Depth over the Northeastern United States during the Summer of 1995, *Journal of Applied Meteorology*, 38(12):1661-1673, [https://doi.org/10.1175/1520-0450\(1999\)038<1661:SATVIT>2.0.CO;2](https://doi.org/10.1175/1520-0450(1999)038<1661:SATVIT>2.0.CO;2), 1999.
- Brattich, E., Orza, J.A.G., Cristofanelli, P., Bonasoni, P., Tositti, L.: Influence of stratospheric air masses on radiotracers and ozone over the central Mediterranean, *J. Geophys. Res.: Atmosphere*, <https://doi.org/10.1002/2017JD027036>, 2017.
- 430 Crawford, J. H., Davis, D. D., Chen, G., Buhr, M., Oltmans, S., Weller, R., Mauldin, L., Eisele, F., Shetter, R., Lefer, B., Arimoto, R., Hogan, A.: Evidence for photochemical production of ozone at the South Pole surface, *Geophysical Research Letters*, 28(19), 3641-3644, <https://doi.org/10.1029/2001gl013055>, 2001.
- Cristofanelli, P., Bonasoni, P., Calzolari, F., Bonafè, U., Lanconelli, C., Lupi, A., Trivellone, G., Vitale, V., Petkov, B.: Analysis of near-surface ozone variations in terra nova bay, Antarctica, *Antarctic Science*, 20(04), 415-421, <http://dx.doi.org/10.1017/S0954102008001028>, 2008.
- 435 Cristofanelli, P., Calzolari, F., U. BONAFÈ, Lanconelli, C., Lupi, A., & Busetto, M.: Five-year analysis of background carbon dioxide and ozone variations during summer seasons at the mario zucchelli station (antarctica), *Tellus. Series B: Chemical and Physical Meteorology*, 63(5), 831-842, <https://doi.org/10.1111/j.1600-0889.2011.00576.x>, 2011.
- 440 Cristofanelli, P., Putero, D., Bonasoni, P., Busetto, M., Calzolari, F., Camporeale, G., Paolo , C., Giuseppe, L., Angelo, P., Boyan, T., Rita, U., Roberto, V.: Analysis of multi-year near-surface ozone observations at the wmo/gaw “concordia” station (75°06’s, 123°20’e, 3280m a.s.l. – antarctica), *Atmospheric Environment*, 177, 54-63, <https://doi.org/10.1016/j.atmosenv.2018.01.007>, 2018.
- Davis, D. D., Nowak, L. B., Chen, G., Buhr, M., Arimoto, R., Hogan, A., Eisele, F., Mauldin, L., Tanner, D., Shetter, R., Lefer, B., and McMurry, P.: Unexpected high levels of NO observed at South Pole, *Geophys. Res. Lett.*, 28, 3625–3628, 2001.
- 445 Davidson A.: Update on ozone trend in California’s south coast air basin, *Journal of the Air & Waste Management Association*, 43, 226–227, <https://doi.org/10.1080/1073161x.1993.10467130>, 1993.
- Dimitriou, K., Kassomenos, P.: Three year study of tropospheric ozone with back trajectories at a metropolitan and a medium scale urban area in Greece, *Sci. Total Environ.*, 502, 493–501, <https://doi.org/10.1016/j.scitotenv.2014.09.072>, 2015.

- Ding, M., Tian, B.: The surface ozone observation data of Kunlun station in 2016 [Data set], Zenodo, <http://doi.org/10.5281/zenodo.3923517>, 2020.
- 450 Draxler, R. R., Rolph, G. D.: HYSPLIT (HYbrid Single-Particle Lagrangian Integrated Trajectory) Model, NOAA Air Resour, Lab., Silver Spring, Md. (Available at <http://www.arl.noaa.gov/ready/hysplit4.html>), 2003.
- Fiebig, M., Hirdman, D., Lunder, C. R., Ogren, J. A., Solberg, S., Stohl, A., and Thompson, R. L.: Annual cycle of Antarctic baseline aerosol: controlled by photooxidation-limited aerosol formation, *Atmos. Chem. Phys.*, 14, 3083–3093, <https://doi.org/10.5194/acp-14-3083-2014>, 2014.
- 455 Frey, M. M., Roscoe, H. K., Kukui, A., Savarino, J., France, J. L., King, M. D., Legrand, M., Preunkert, S.: Atmospheric nitrogen oxides (NO and NO₂) at Dome C, East Antarctica, during the OPALE campaign, *Atmos. Chem. Phys.* 15(14), 7859-7875. <https://doi.org/10.5194/acp-15-7859-2015>, 2015.
- Fishman J, Brackftt V G, Fakhruzzaman K.: Distribution of tropospheric ozone in the tropics from satellite and ozonesonde measurements, *Journal of Atmospheric & Terrestrial Physics*, 54(5):589-597, 1992.
- 460 Giostra, U., Furlani, F., Arduini, J., Cava, D., Manning, A., O'Doherty, S., Reimann, S., Maione, M.: The determination of a “regional” atmospheric background mixing ratio for anthropogenic greenhouse gases: a comparison of two independent methods, *Atmos. Environ.* 45, 7396–7405, <https://doi.org/10.1016/j.atmosenv.2011.06.076>, 2011.
- Greenslade, J. W., Alexander, S. P., Schofield, R., Fisher, J. A., and Klekociuk, A. K.: Stratospheric ozone intrusion events and their impacts on tropospheric ozone in the Southern Hemisphere, *Atmos. Chem. Phys.*, 17, 10269–10290, 465 <https://doi.org/10.5194/acp-17-10269-2017>, 2017.
- Gruzdev, A. N., Sitnov, S. A.: Tropospheric ozone annual variation and possible troposphere-stratosphere coupling in the arctic and antarctic as derived from ozone soundings at resolute and amundsen-scott stations, *Tellus. Series B: Chemical and Physical Meteorology*, 45(2), 89-98, <https://doi.org/10.1034/j.1600-0889.1993.t01-1-00001.x>, 1993.
- Ghude, S. D., Kumar, A., Jain, S. L., Arya, B. C., Bajaj, M. M.: Comparative study of the total ozone column over maitri, 470 antarctica during 1997, 2002 and 2003, *International Journal of Remote Sensing*, 26(16), 3413-3421, <https://doi.org/10.1080/01431160500076434>, 2005.
- Hara, K., Osada, K., Nishita-Hara, C., and Yamanouchi, T.: Seasonal variations and vertical features of aerosol particles in the Antarctic troposphere, *Atmospheric Chemistry and Physics*, 11(11), 5471-5484, <https://doi.org/10.5194/acp-11-5471-2011>, 2011.

- 475 Helmig, D. , Johnson, B. , Samuel, J. , Oltmans, Neff, W. , Eisele, F.: Elevated ozone in the boundary layer at south pole, Atmospheric environment, 42(12), p.2788-2803, <https://doi.org/10.1016/j.atmosenv.2006.12.032>, 2008a.
- Helmig, D. , Johnson, B. J. , Warshawsky, M. , Morse, T. , Neff, W. D. , Eisele, F.: Nitric oxide in the boundary-layer at south pole during the antarctic tropospheric chemistry investigation (antci), Atmospheric Environment, 42(12), <https://doi.org/2817-2830,10.1016/j.atmosenv.2007.03.061>, 2008b.
- 480 Honrath, R. E., Guo, S., Peterson, M. C., Dziobak, M. P., Dibb, J. E., and Arsenault, M. A.: Photochemical production of gas phase NO_x from ice crystal NO₃⁻, Journal of Geophysical Research: Atmospheres, 105(D19), 24183-24190, <https://doi.org/10.1016/j.10.1029/2000JD900361,2000a>.
- Honrath, R. E., Peterson, M. C., Dziobak, M. P., Dibb, J. E., Arsenault, M. A., and Green, S. A.: Release of NO_x from sunlight-irradiated midlatitude snow, Geophysical Research Letters, 27(15), 2237-2240, <https://doi.org/10.1029/1999GL011286>,
485 2000b.
- Hopke, P.K., Barrie, L.A., Li, S.-M., Cheng, M.-D., Li, C., Xie, Y.: Possible sources and preferred pathways for biogenic and non-sea-salt sulfur for the high Arctic. J. Geophys. Res.: Atmosphere 100, 16595–16603, <https://doi.org/10.1029/95JD01712>, 1995.
- IPCC. Summary for policymakers[M] // Climate Change 2013: The Physical Science Basis. Contribution of Working Group to
490 the fifth assessment report of the Intergovernmental Panel on Climate Change. Cambridge & New York: Cambridge University Press, 2013.
- Jones, A. E., Weller, R., Wolff, E. W., and Jacobi, H. W.: Speciation and rate of photochemical NO and NO₂ production in Antarctic snow, Geophysical Research Letters, 27(3), 345-348, <https://doi.org/10.1029/1999GL010885>, 2000.
- Jones, A.E., Wolff, E.W.: An analysis of the oxidation potential of the South Pole boundary layer and the influence of
495 stratospheric ozone depletion, Journal of Geophysical Research, 108(D18):4565, <https://doi.org/10.1029/2003JD003379>, 2003.
- Johnson T., Capel J., Ollison W.: Measurement of microenvironmental ozone concentrations in Durham, North Carolina, using a 2B Technologies 205 Federal Equivalent Method monitor and an interference-free 2B Technologies 211 monitor, Journal of the Air & Waste Management Association, 64(3):360-371, <https://doi.org/10.1080/10962247.2013.839968>,
500 2014.
- Kaiser, A., Scheifinger, H., Spangl, W., Weiss, A., Gilge, S., Fricke, W., Ries, L., Cemas, D., and Jesenovec, B.: Transport of nitrogen oxides, carbon monoxide and ozone to the alpine global atmosphere watch stations Jungfrauoch (Switzerland),

Zugspitze and Hohenpeißenberg (Germany), Sonnblick (Austria) and Mt.Krvavec (Slovenia), *Atmos. Environ.*, 41, 9273–9287, <https://doi.org/10.1016/j.atmosenv.2007.09.027>, 2007.

505 Lawrence, J. S., Ashley, M. C. B., Hengst, S., Luong-Van, D. M., Storey, J. W. V., Yang, H., Zhou, X., and Zhu, Z.: *The PLATO Dome A site testing observatory: power generation and control systems*, *Review of Scientific Instruments*, 80, 064501-1–064501-10, 2009.

Legrand, M., Preunkert, S., Jourdain, B., Gallée, H., Goutail, F., Weller, R., and Savarino, J.: Year-round record of surface ozone at coastal (Dumont d'Urville) and inland (Concordia) stations in East Antarctica, *Journal of Geophysical Research: Atmospheres*, 114(D20), <https://doi.org/10.1029/2008JD011667>, 2009.

510 Lei B., Min L.: Discussion on Maintenance of O₃42M type Automatic Ozone Analyzer, *Environmental Science Survey*, 2014.

Legrand, M., Preunkert, S., Savarino, J., Frey, M.M., Kukui, A., Helmig, D., Jourdain, B., Jones, A.E., Weller, R., Brough, N., Gallée, H.: Inter-annual variability of surface ozone at coastal (Dumont d'Urville, 2004–2014) and inland (Concordia, 2007–2014) sites in East Antarctica, *Atmos. Chem. Phys.* 16, 8053–8069. <http://dx.doi.org/10.5194/acp-16-8053-2016>, 2016.

Liang, F., Cunde, X., Lingen, B.: Vertical Structure of Atmosphere on East Antarctic Plateau, *Plateau Meteorology*, 2015.

Lin, C., Gillespie, J., Schuder, M. D., Duberstein, W., Beverland, I. J., Heal, M. R.: Evaluation and calibration of aerqual series 500 portable gas sensors for accurate measurement of ambient ozone and nitrogen dioxide, *Atmospheric Environment*, 100, 111-116, <http://dx.doi.org/10.1016/j.atmosenv.2014.11.002>, 2015.

520 Lin, M., Horowitz, L. W., Payton, R., Fiore, A. M., and Tonnesen, G.: US surface ozone trends and extremes from 1980 to 2014: quantifying the roles of rising Asian emissions, domestic controls, wildfires, and climate, *Atmos. Chem. Phys.*, 17, 2943– 2970, <https://doi.org/10.5194/acp-17-2943-2017>, 2017.

Liu, J., Zhang, X. L., Zhang, X. C., Tang, J.: Surface Ozone Characteristics and the Correlated Factors at Shangdianzi Atmospheric Background Monitoring Station, *Research of Environmental Sciences*, [https://doi.org/10.1016/S1872-2040\(06\)60041-8](https://doi.org/10.1016/S1872-2040(06)60041-8), 2006.

Mickley, L. J., Murti, P. P., Jacob, D. J., Logan, J. A., Koch, D. M., and Rind, D.: Radiative forcing from tropospheric ozone calculated with a unified chemistry-climate model, *Journal of Geophysical Research: Atmospheres*, 104(D23), 30153-30172, <https://doi.org/10.1029/1999JD900439>, 1999.

- 530 Mihalikova, M., Kirkwood, S.: Tropopause fold occurrence rates over the Antarctic station Troll (72°S, 2.5°E), *Ann. Geophys.* 31, 591–598. <http://dx.doi.org/10.5194/angeo-31-591-2013>, 2013.
- Monks, P. S., Archibald, A. T., Colette, A., Cooper, O., Coyle, M., Derwent, R., Fowler, D., Granier, C., Law, K. S., Mills, G. E., Stevenson, D. S., Tarasova, O., Thouret, V., von Schneidmesser, E., Sommariva, R., Wild, O., and Williams, M. L.: Tropospheric ozone and its precursors from the urban to the global scale from air quality to short-lived climate forcer, *Atmos. Chem. Phys.*, 15, 8889–8973, <https://doi.org/10.5194/acp-15-8889-2015>, 2015.
- 535 Moura, Bárbara Bâesso, Souza, Sílvia Ribeiro de, Alves E S: Respostas estruturais em *Ipomoea nil* (L.) Roth 'Scarlet O'Hara' (Convolvulaceae) exposta ao ozônio, *Acta Botanica Brasilica*, 25(1):122-129, <https://doi.org/10.1590/S0102-33062011000100015>, 2011.
- Murayama, S., Nakazawa, T., Tanaka, M., Aoki, S., Kawaguchi, S.: Variations of tropospheric ozone concentration over Syowa Station, Antarctica, *Tellus B* 44, 262–272, <http://dx.doi.org/10.1034/j.1600-0889.1992.t01-3-00004.x>, 1992.
- 540 Nadzir, M., Ashfold, M., Khan, M., et al.: Spatial-temporal variations in surface ozone over Ushuaia and the Antarctic region: observations from in situ measurements, satellite data, and global models, *Environmental Science & Pollution Research*, <http://dx.doi.org/10.1007/s11356-017-0521-1>, 2018.
- Neff, W., Helmig, D., Grachev, A., Davis, D.: A study of boundary layer behavior associated with high NO concentrations at the south pole using a minisodar, tethered balloon, and sonic anemometer, *Atmospheric Environment*, 42(12), 2762-2779, <http://dx.doi.org/10.1016/j.atmosenv.2007.01.033>, 2008a.
- 545 Neff, W., Perlwitz, J., Hoerling, M.: Observational evidence for asymmetric changes in tropospheric heights over Antarctica on decadal time scales, *Geophysical Research Letters*, 35(18), 102-102, <http://dx.doi.org/10.1029/2008GL035074>, 2008b.
- Oltmans, S. J., Komhyr, W. D.: Surface ozone in Antarctica, *Journal of Geophysical Research*, v. 81, p. 5359-5364. <http://dx.doi.org/10.1029/jc081i030p05359>, 1976.
- 550 Oltmans, S. J., Johnson, B. J., & Helmig, D.: Episodes of high surface-ozone amounts at south pole during summer and their impact on the long-term surface-ozone variation, *Atmospheric Environment*, 42(12), 2804-2816, <https://doi.org/10.1016/j.atmosenv.2007.01.020>, 2008.
- Polissar, A., Hopke, P., Paatero, P., Kaufmann, Y., Hall, D., Bodhaine, B., Dutton, E., and Harris, J.: The aerosol at Barrow, Alaska: long-term trends and source locations, *Atmos. Environ.*, 33, 2441–2458, [https://doi.org/10.1016/S1352-2310\(98\)00423-3](https://doi.org/10.1016/S1352-2310(98)00423-3), 1999.
- 555

- Prados-Roman C, Gómez L, Puentedura O, et al. Ground-based observations of Halogen Oxides in the Antarctic Boundary Layer[C]//EGU General Assembly Conference Abstracts. 2017, 19: 11798.
- 560 Putero, D., Cristofanelli, P., Sprenger, M., Škerlak, B., Tositti, L., and Bonasoni, P.: STEFLUX, a tool for investigating stratospheric intrusions: application to two WMO/GAW global stations, *Atmos. Chem. Phys.*, 16, 14203-14217, <https://doi.org/10.5194/acp-16-14203-2016>, 2016.
- Robinson, E., Clark, D., Cronn, DR.: Stratospheric-tropospheric Ozone Exchange in Antarctica Caused By Mountain Waves, *Journal of Geophysical Research Oceans*, 88(C15): 10708-10720, <https://doi.org/10.1029/JC088iC15p10708>, 1983.
- 565 Roscoe H K.: Possible descent across the “Tropopause” in Antarctic winter, *Advances in Space Research*, 33(7):1048-1052, [https://doi.org/10.1016/S0273-1177\(03\)00587-8](https://doi.org/10.1016/S0273-1177(03)00587-8), 2004.
- Sagona J A., Weisel C P., Meng Q.: Accuracy and practicality of a portable ozone monitor for personal exposure estimates, *Atmospheric Environment*, 175(FEB.):120-126, <https://doi.org/10.1016/j.atmosenv.2017.11.036>, 2018, .
- Schnell, R. C., Liu, S. C., Oltmans, S. J., Stone, R. S., Hofmann, D. J., Dutton, E. G.: Decrease of summer tropospheric ozone concentrations in antarctica, *Nature*, 351(6329), 726-729, <https://doi.org/10.1038/351726a0>, 1991.
- 570 Škerlak, B., Sprenger, M., and Wernli, H.: A global climatology of stratosphere–troposphere exchange using the ERA-Interim data set from 1979 to 2011, *Atmos. Chem. Phys.*, 14, 913-937, <https://doi.org/10.5194/acp-14-913-2014>, 2014.
- Slusher, D. L., Neff, W. D., Kim, S., Huey, L. G., Wang, Y., Zeng, T., Tanner, D. J., Blake, D. R., Beyersdorf, A., Lefer, B. L., Crawford, J. H., Eisele, F. L., Mauldin, R. L., Kosciuch, E., Buhr, M. P., Wallace, H. W., and Davis, D. D.: Atmospheric chemistry results from the ANTCI 2005 Antarctic plateau airborne study. *Journal of Geophysical Research: Atmospheres*, 115(D7), <https://doi.org/10.1029/2009JD012605>, 2010.
- 575 Sprovieri, F., Pirrone, N., Gaerdfeldt, K., Sommar, J.: Mercury speciation in the marine boundary layer along a 6000 km cruise path around the Mediterranean Sea, *Atmospheric Environment*, 37(1):63-71, [https://doi.org/10.1016/S1352-2310\(03\)00237-1](https://doi.org/10.1016/S1352-2310(03)00237-1), 2003.
- Stevenson, D. S., Johnson, C. E., Collins, W. J., Derwent, R. G., Shine, K. P., and Edwards, J. M.: Evolution of tropospheric ozone radiative forcing, *Geophysical Research Letters*, 25(20), 3819-3822, <https://doi.org/10.1029/1998GL900037>, 1998.
- 580 Stohl, A., Sodemann, H.: Characteristics of atmospheric transport into the Antarctic troposphere, *J. Geophys. Res.: Atmosphere* 115, D02305. <http://dx.doi.org/10.1029/2009JD012536>, 2010

- Traversi, R., Udisti, R., Frosini, D., Becagli, S., Ciardini, V., Funke, B., Lanconelli, C., Petkov, B., Scarchilli, C., Severi, M.,
585 Vitale, V.: Insights on nitrate sources at Dome C (East Antarctic Plateau) from multi-year aerosol and snow records,
Tellus, B66, 22550, <https://doi.org/10.3402/tellusb.v66.22550>, 2014.
- Traversi, R., Becagli, S., Brogioni, M., Caiazzo, L., Ciardini, V., Giardi, F., Legrand, M., Macelloni, G., Petkov, B., Preunkert,
S., Scarchilli, C., Severi, M., Vitale, V., Udisti, R.: Multi-year record of atmospheric and snow surface nitrate in the
central Antarctic plateau. *Chemosphere* 172, 341–354,
590 <http://www.sciencedirect.com/science/article/pii/S0045653516318872>, 2017.
- Wakamatsu, S., Ohara, T., and Uno, I.: Recent trends in precursor concentrations and oxidant distributions in the Tokyo and
Osaka areas, *Atmospheric Environment*, 30(5), 715-721, [https://doi.org/10.1016/1352-2310\(95\)00274-X](https://doi.org/10.1016/1352-2310(95)00274-X), 1996.
- Wang, S J., Tian, B., Ding, M H., Zhang, D Q., Zhang,T., Sun, W J.: Usage and performance assessment of a novel O₃
analyzer-model 205, *OPTICAL INSTRUMENTS*, 039(002), 58-63, 88,
595 <https://doi.org/10.3969/j.issn.1005-5630.2017.02.011>, 2017.
- Wang Y T., Bian L G., Ma Y F., Tang J., Zhang D Q., Zheng X D.: Surface ozone monitoring and background characteristics
at Zhongshan Station over Antarctica. *Chinese Sci Bull*, 56(11), 848-857., <https://doi.org/10.1007/s11434-011-4406-2>,
2011.
- Wang, Y. Q.: MeteoInfo: GIS software for meteorological data visualization and analysis, *Meteorological Applications*, 21(2),
600 360-368, <https://doi.org/10.1002/met.1345>, 2014.
- Wong, JAHA.: Algorithm AS 136: A K-Means Clustering Algorithm, *Journal of the Royal Statistical Society*, 28:100-108,
<https://doi.org/10.2307/2346830>, 1979.
- Xu, W., Xu, X., Lin, M., Lin, W., Tarasick, D., Tang, J., Ma, J., and Zheng, X.: Long-term trends of surface ozone and its
influencing factors at the Mt Waliguan GAW station, China – Part 2: The roles of anthropogenic emissions and
605 climate variability, *Atmos. Chem. Phys.*, 18, 773–798, <https://doi.org/10.5194/acp-18-773-2018>, 2018.
- Ye, L., Bian, L., Tang, J., Ding, M., Zheng, X., Gao, Z.: A study on surface ozone depletion episodes over the A ntarctic
coast, *Acta Meteorologica Sinica*, 75(3), 506-516, <https://doi.org/10.11676/qxxb2017.027>, 2017.
- Yin, X., Kang, S., de Foy, B., Cong, Z., Luo, J., Zhang, L., Ma, Y., Zhang, G., Rupakheti, D., and Zhang, Q.: Surface ozone at
Nam Co in the inland Tibetan Plateau: variation, synthesis comparison and regional representativeness, *Atmos. Chem.*
610 *Phys.*, 17, 11293-11311, <https://doi.org/10.5194/acp-17-11293-2017>, 2017.

615

620

625

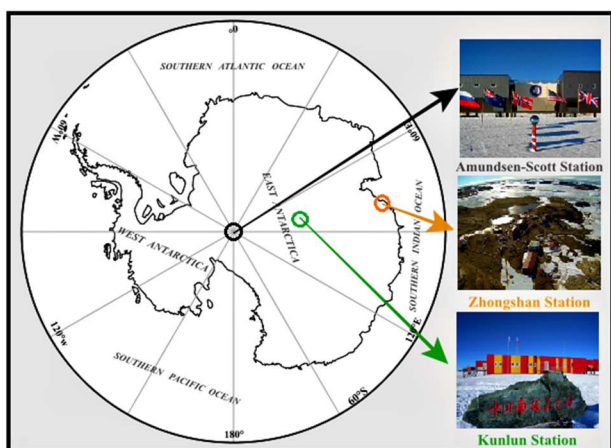


Figure 1: Amundsen-Scott Station (South Pole, SP), Kunlun Station (Dome A, DA) and Zhongshan Station (ZS) locations in Antarctica.

Table 1. The calibration record of ozone monitor

Date	Span Point (ppb)	Thermo 49ips (ppb)	Model 205 (ppb)
2015/10/5	0	-0.79	0.26
	20	19.99	20.73
	35	34.99	35.35
	50	50.02	50.73
	65	64.96	65.71
	80	79.99	80.48
	100	99.99	100.43
	120	119.96	120.31
2017/5/6	0	-0.71	0.51
	20	20.00	21.68
	35	34.95	36.95
	50	50.01	52.17
	65	64.98	67.37
	80	79.99	82.88
	100	100.00	103.00
	120	119.92	124.10

630

635 **Table 2. Stability test of ozone monitor.**

Time	Slope	Standard Uncertainty	Intercept	Standard Uncertainty
2015/10/5	0.99936	0.00195	0.53861	0.13672
2017/5/6	1.02520	0.00264	0.85220	0.18491
Average	1.01228	0.00230	0.69541	0.16082
Standard Error	0.01827	0.00049	0.22174	0.03408

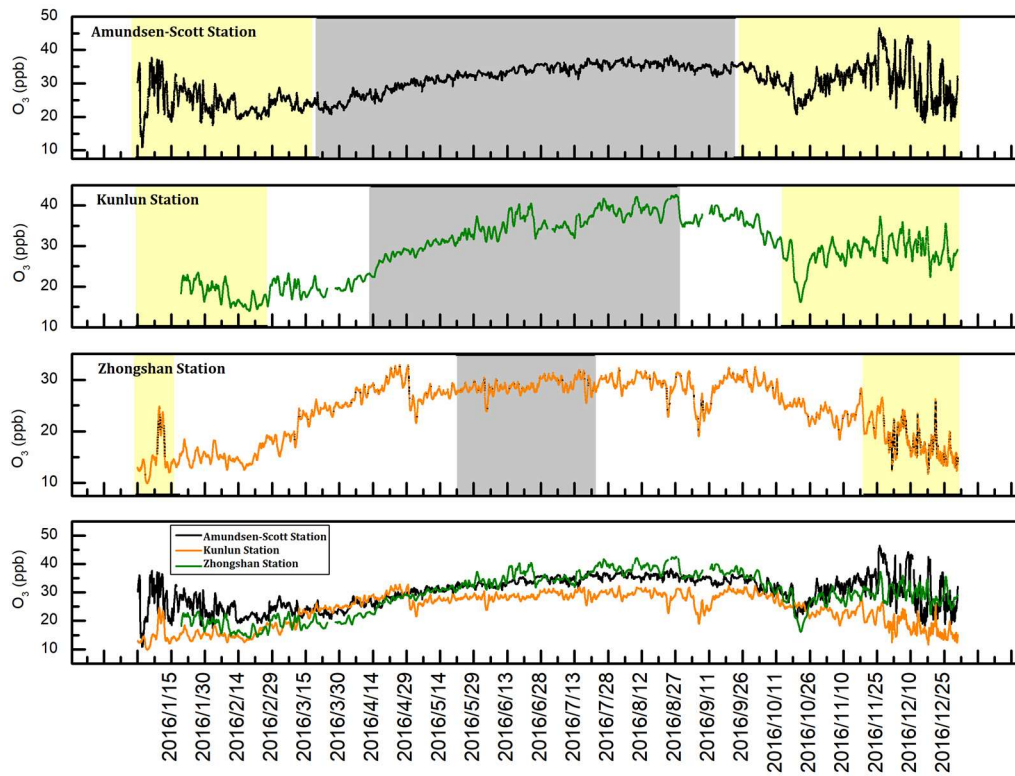
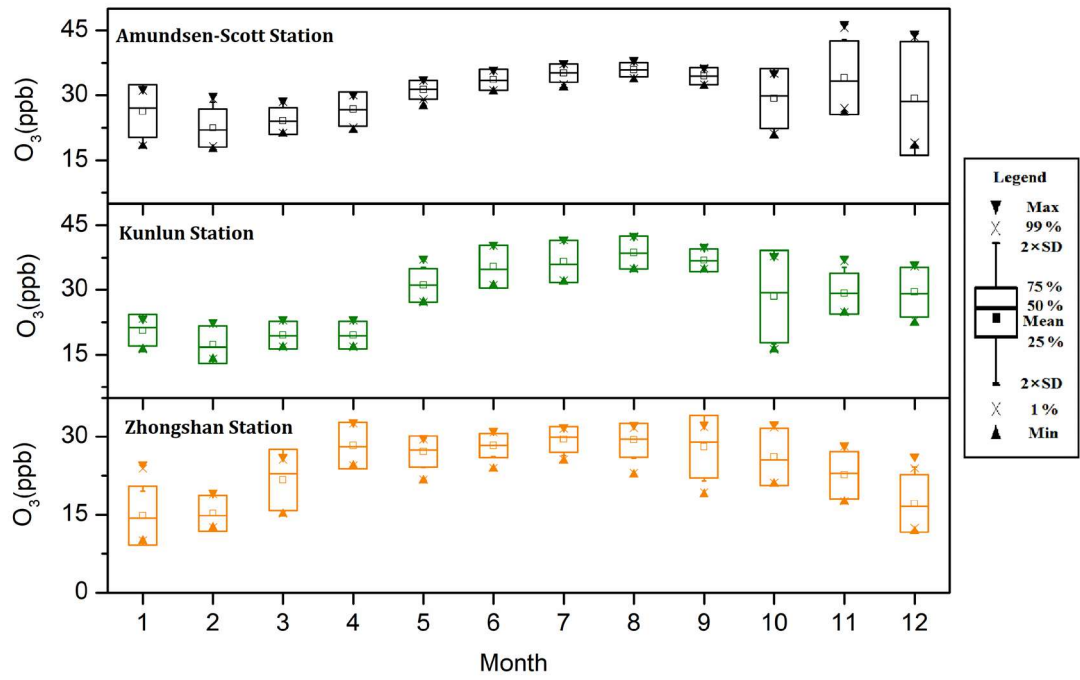


Figure 2: Time series of near-surface O₃ at the SP, DA and ZS during 2016. Yellow (grey) shading identifies polar day (night).



640

Figure 3: Monthly average and statistical parameters of near-surface O₃ at the SP, DA and ZS during 2016.

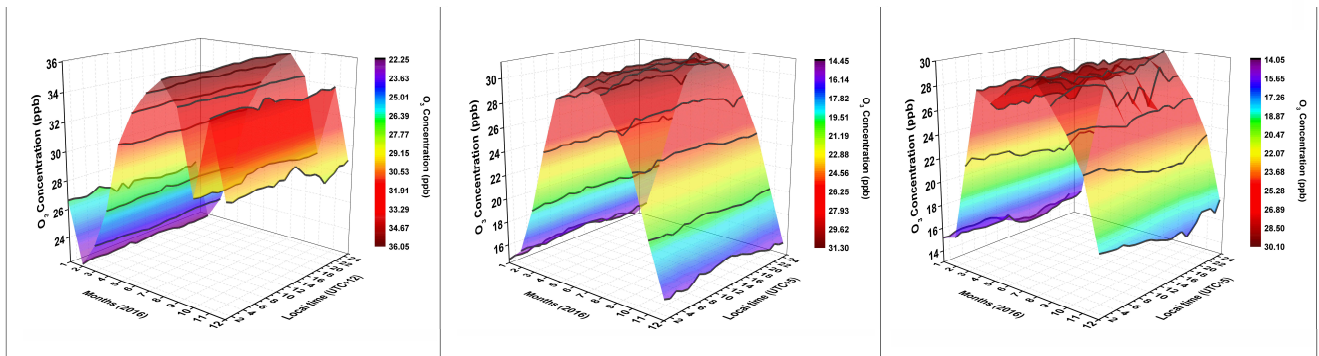
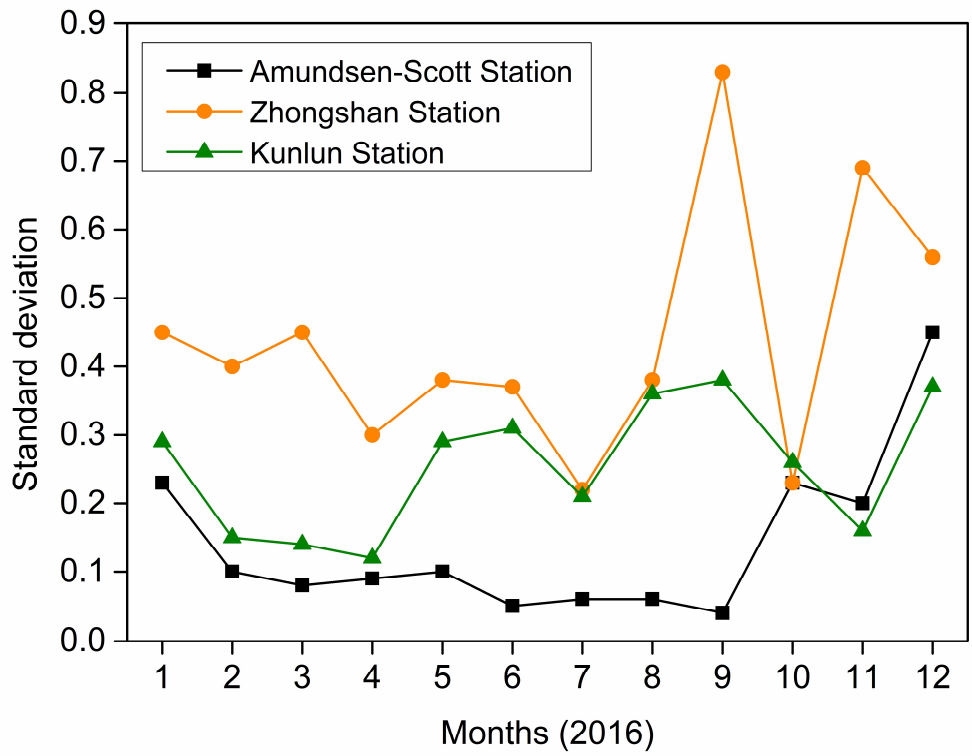


Figure 4: Mean diurnal variations in near-surface O₃ concentrations at the SP (a), DA (b) and ZS (c) during 2016.



645 **Figure 5: Standard deviations of mean diurnal variation in near-surface O₃ concentrations at the SP, DA and ZS during 2016.**

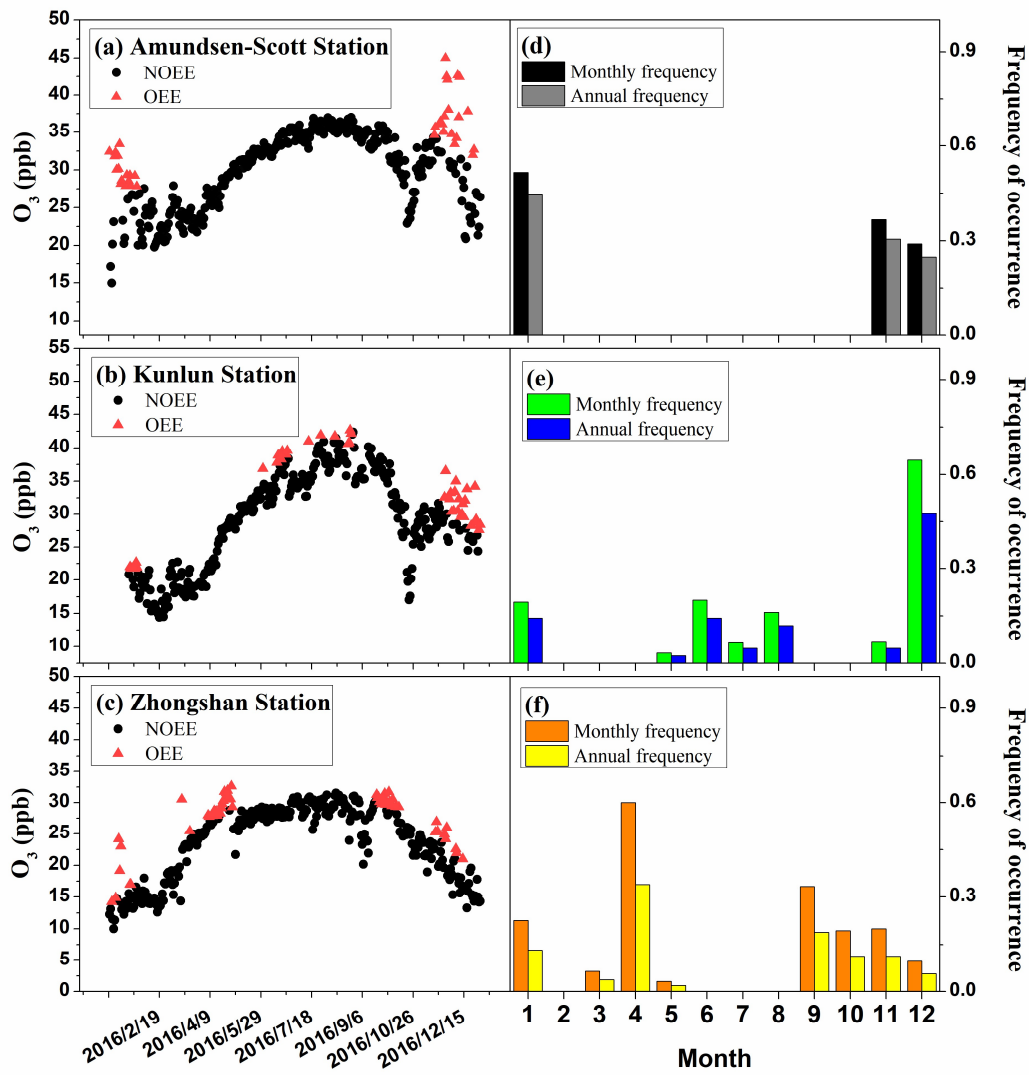


Figure 6: (a, b and c) The OEEs and (d, e and f) averaged distribution of OEE occurrence among the different months of 2016 at the three stations. $Monthly\ frequency = \frac{\text{number of OEE days for each month}}{\text{number of days in the month}}$; $Annual\ frequency =$

650 $\frac{\text{number of OEE days for each month}}{\text{total number of OEE days}}$.

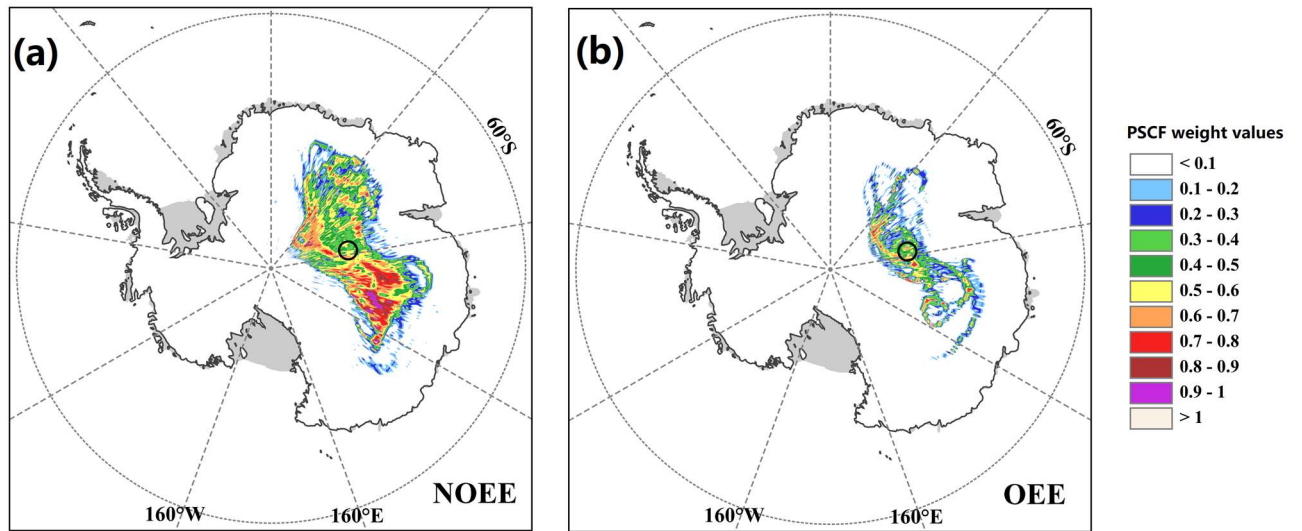
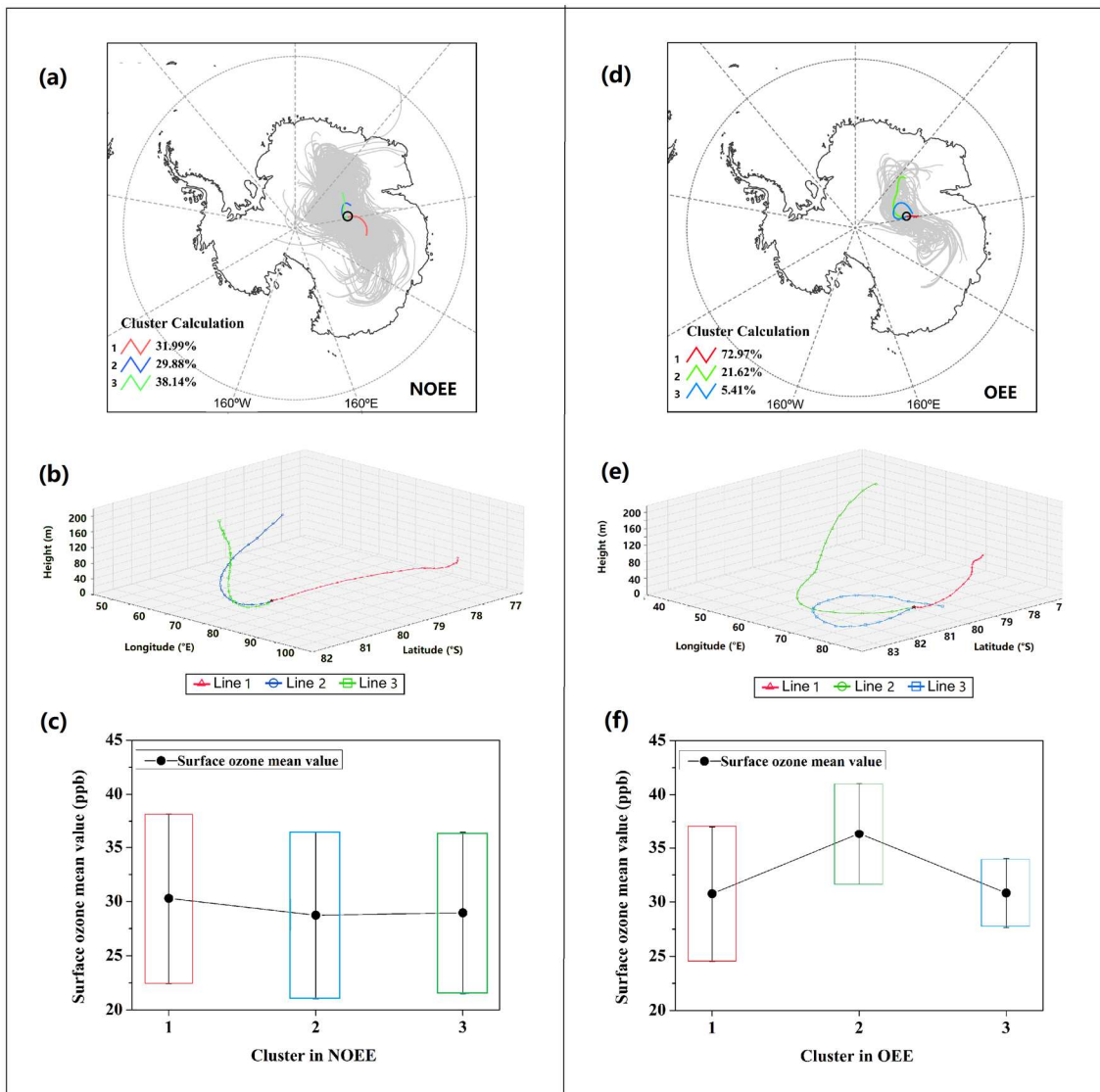


Figure 7: Likely source areas of surface O_3 at Kunlun Station during the NOEE (a) and OEE (b) identified using the PSCF (Potential Source Contribution Function).



655

Figure 8: Backward HYSPLIT trajectories for each measurement day (gray lines in Figure 8a), and mean back trajectory for 3 HYSPLIT clusters (colored lines in Figure 8a, 3D view shown in Figure 8b) arriving at Kunlun Station during NOEEs. Subplot (c) shows the range of surface ozone concentrations measured at DA by cluster. Error bar is the standard deviation of the same cluster. Same as subplot (a, b, c), but subplot (d, e, f) for OEEs.

660

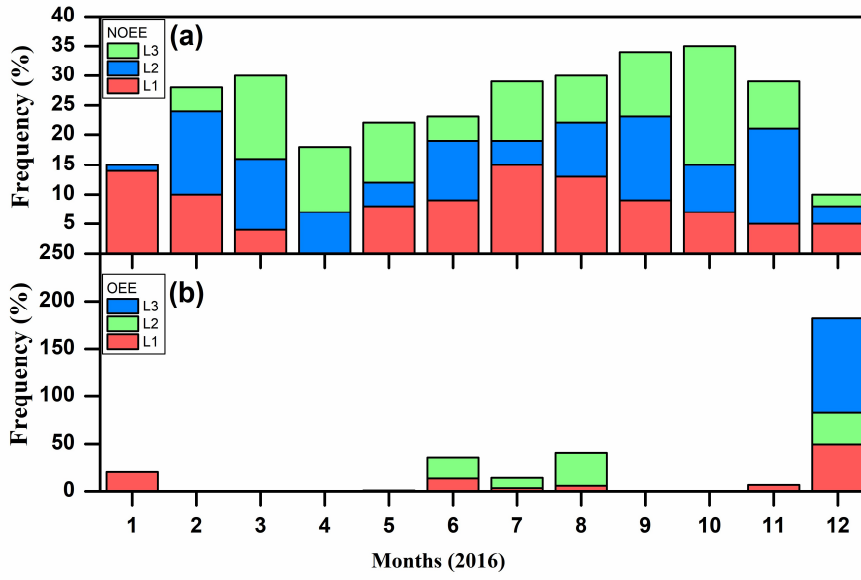
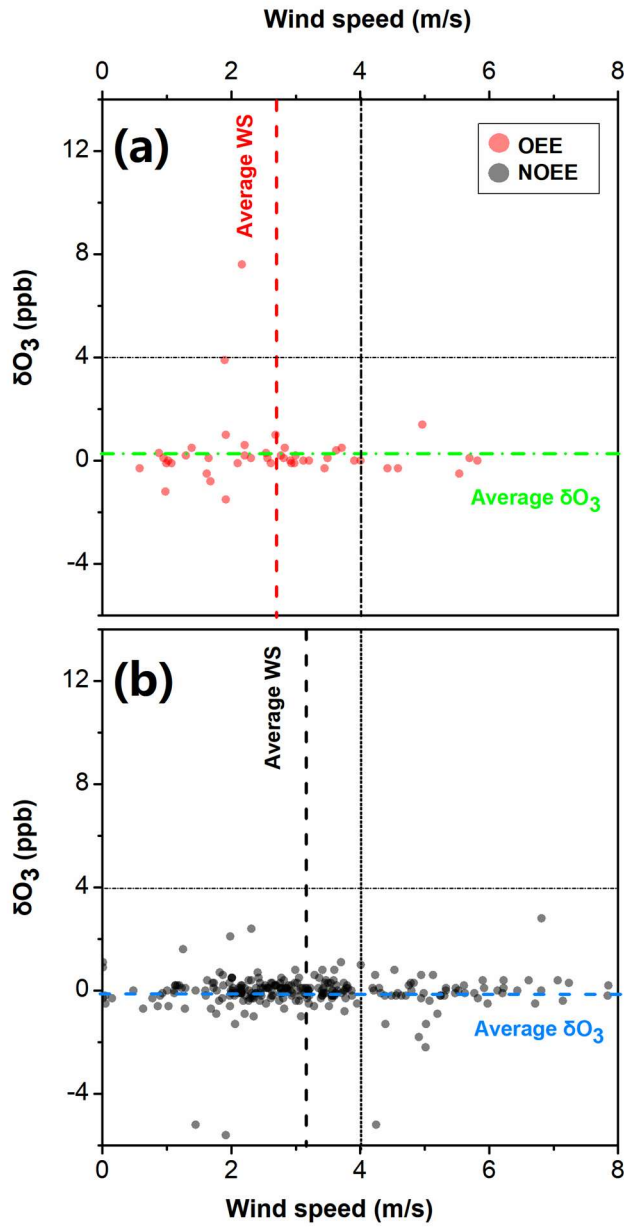
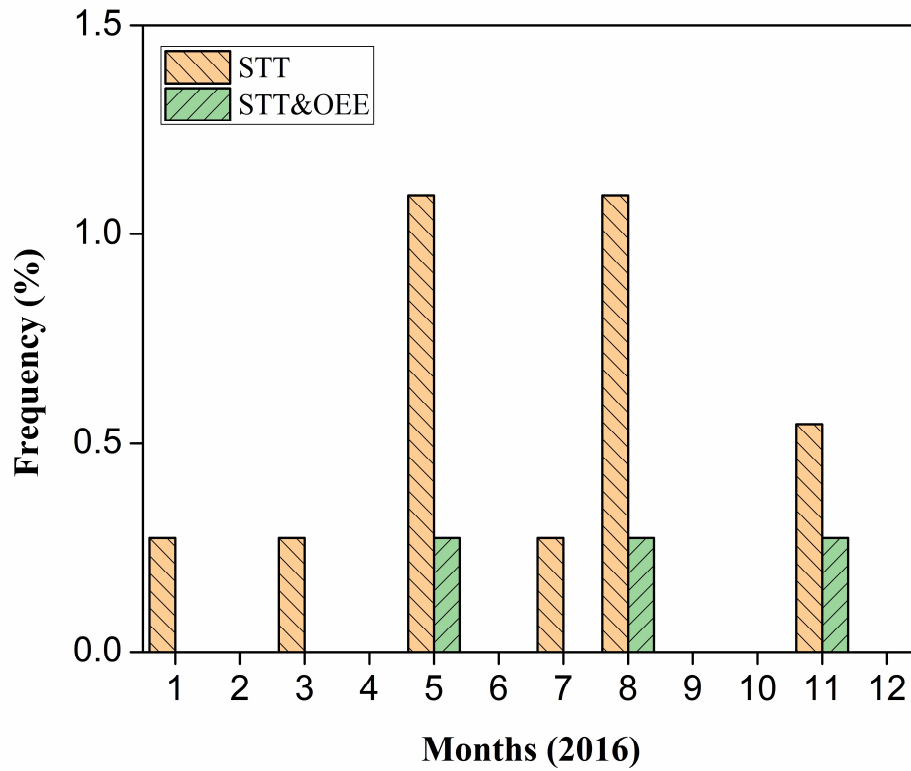


Figure 9: Monthly frequency distribution of clustering trajectories (Line 1, 2, 3) during NOEEs and OEEs.



665 **Figure 10: Wind speed and ΔO_3 statistical distribution around OEEs (red dots) and NOEEs (black dots) at DA in polar night. Here, ΔO_3 represents the growth rate of near-surface O_3 concentration, calculated by equation:**

$$\Delta O_3 = \frac{\text{The } O_3 \text{ concentration at } T_n - \text{The } O_3 \text{ concentration at } T_{n-1}}{\text{Time difference of } T_n \text{ and } T_{n-1}}$$



670 Figure 11: Annual variation of “deep” STT events at Kunlun Station and the annual variation of it occurred at the same time with OEE over the period 2016, obtained by STEFLUX.